Concurrent Photocatalytic Hydrogen Generation and Dye Degradation Using MIL-125-NH_2 under Visible Light Irradiation

Stavroula Kampouri,[a] Tu N. Nguyen,[a] Mariana Spodaryk,[b] Robert G. Palgrave,[c] Andreas Züttel,[b] Berend Smit,[a] Kyriakos C. Stylianou[a]*

a. Laboratory of Molecular Simulation (LSMO), b. Laboratory of Materials for Renewable Energy (LMER), Institute of Chemical Sciences and Engineering (ISIC), Ecole Polytechnique Fédérale de Lausanne (EPFL Valais) Rue de l'industrie 17, 1951 Sion (Switzerland)
c. University College London, Department of Chemistry, 20 Gordon St., London, WC1H 0AJ, UK

* **Corresponding Author**

kyriakos.stylianou@epfl.ch

Abstract. Herein, we first systematically studied the impact of different transition metal-based co-catalysts towards the photocatalytic water reduction, when they are physically mixed with the visible-light active MIL-125-NH_2. All co-catalyst/MIL-125-NH_2 photocatalytic systems were found to be highly stable after photocatalysis, with the NiO/MIL-125-NH_2 and Ni_2P/MIL-125-NH_2 systems exhibiting high hydrogen (H_2) evolution rates of 1084 and 1230 $\mu mol\ h^{-1}\ g^{-1}$, respectively. Secondly, we investigated how different electron donors affected the stability and H_2 generation rate of the best Ni_2P/MIL-125-NH_2 system and found that triethylamine fulfils both requirements. We then replaced the electron donor with rhodamine

1

B (RhB), a dye that is commonly used as a simulant organic pollutant, with the aim of integrating the photocatalytic H_2 generation with the degradation of RhB in a single process. This is of supreme importance as by replacing the costly (and toxic) electron donors with hazardous molecules present in waste water, makes it possible to oxidise organic pollutants and produce H_2 simultaneously. This is the first study where a metal-organic framework (MOF) system is used for this dual-photocatalytic activity under visible light illumination and our proof-of-concept approach envisions a sustainable waste-water remediation process driven by the abundant solar energy, while H_2 is produced, captured and further utilized.

1. Introduction

Photocatalysis is a process in which a photoactive material (photosensitizer/photocatalyst) is excited upon light irradiation, generating electron-hole pairs that can be eventually involved in a variety of chemical reactions.[1] Solar-driven hydrogen (H_2) evolution from water splitting and photocatalytic remediation of contaminated water are two of the major areas in the general field of photocatalysis that have received tremendous attention during the last few decades.[2] Extensive research in water splitting was triggered by the urgent need for renewable energy resources to replace fossil fuels, which have been the main source of air pollution, carbon dioxide (CO_2) and other greenhouse gases emissions.[3] H_2 gas produced from water splitting is considered a clean energy carrier for a sustainable energy future, since it offers a high energy density whilst the outcome of the H_2 combustion is water, allowing for an energy cycle free of greenhouse gases.[4] Considerable efforts have also been devoted to photocatalytic water remediation in which contaminants such as organic dyes and polyaromatic hydrocarbons are degraded into CO_2 and H_2O.[5] Water pollution due to human activities is one of the most serious contemporary environmental problems. The continuously increasing production of waste water, along with the severe water scarcity predicted for the near future indicates that there is an urgent need for the development of systems and

techniques that can efficiently ameliorate waste water and prevent the polluted water having an irreversible effect on the environment.[6]

Photocatalytic water splitting and water remediation often employ semiconductors, e.g. TiO_2, as the photocatalyst and the principles of these reactions are well understood.[7] In water splitting, upon irradiation, the photogenerated electrons of the semiconductor are transferred to the catalytic sites of a co-catalyst, which catalyzes the reduction of protons (H^+) or water molecules to H_2. The photogenerated holes in photocatalytic H_2 generation are scavenged by the sacrificial electron donors.[8] In water remediation, several processes can occur simultaneously once the semiconductor has been irradiated: *i.* due to the high oxidizing power of the photogenerated holes, the organic contaminants such as dyes can be oxidized and degraded directly, *ii.* water can be oxidized to form hydroxyl radicals $HO^{\bullet}$, which are highly reactive in the organic dye degradation and *iii.* in the presence of oxygen (O_2) the photogenerated electrons reduce O_2 to a superoxide radical ($O_2^{\bullet-}$), which can also be involved in the degradation process of organic substances.[7],[9]

The great challenges that remain in solar-driven H_2 evolution are to improve the activity of the photocatalytic systems and to minimise the use of expensive (and possibly toxic) electron donors and co-catalysts. The low activity of most photocatalytic systems is often due to the low visible-light absorption of the semiconducting photocatalysts or to their low hydrolytic stability. For example, well-studied semiconductors such as TiO_2 only operate under UV irradiation, which accounts for only 4% of the solar irradiation, while CdS can undergo a high degree of photocorrosion.[10] Co-catalysts are essential for the promotion of the electron-hole separation and the provision of catalytic centers for the reduction of water. The most frequently used co-catalysts are based on expensive noble metals such as Pt nanoparticles (NPs).[11] As mentioned above, the photoexcited holes are usually scavenged by electron donors in order to balance the H_2 generation half reaction;[12] however, many of the electron donors are highly toxic and hazardous (e.g. triethylamine TEA, triethanolamine

TEOA, methanol) or they are an energy resource themselves (e.g. methanol, ethanol), and their introduction substantially increases the cost of the photocatalytic system. Consequently, the requirement for such electron donors is one of the limiting factors hindering the industrial application of such photocatalytic systems.

In order to address these challenges and develop an efficient photocatalytic system, our approach includes:

a. the use of metal-organic frameworks (MOFs) as photocatalysts. MOFs are a class of porous materials consisting of metal ions or clusters coordinated by organic ligands.[13] Their high structural tunability allows the incorporation of visible light-active ligands and reductive metal ions, making them ideal candidates for photocatalytic applications.[1c, 14] In fact numerous photocatalytically active MOFs have been designed or modified through the strategic selection of light-responsive organic ligands, e.g. porphyrins, rhodamine-based, amino-functionalised carboxylate ligands, and metal ions such as Zr(IV) and Ti(IV).[10a, 11c, 15]

b. the employment of earth-abundant co-catalysts as alternatives to noble metal nanoparticles.[4a] It is worth noting that since the number of potential earth-abundant metal oxides or phosphides is essentially limitless, it should be possible to boost the H_2 generation performance of a MOF-based photocatalytic system by simply choosing the right co-catalyst. The overall efficiency of MOF-based photocatalytic systems is substantially determined by the synergy between the MOF photocatalyst and co-catalyst. The key factors for achieving optimal synergy include: *i.* energetic alignment, *ii.* kinetic compatibility and *iii.* morphological match between the MOF crystals and co-catalyst nanoparticles that ensures efficient contact between them and thus a high electron transfer rate.

c. the utilization of contaminated water, with the organic contaminants serving as sacrificial electron donors. With this strategy, the photocatalytic H_2 generation and the water remediation are combined in a single dual-functional system. To date there have been few reports on systems combining the photocatalytic hydrogen evolution with the degradation of

organic compounds, with the UV-active semiconductors (e.g. TiO_2) being the most studied materials.[16]

In the present work, we report for the first time a system that operates under visible light irradiation ($\lambda \geq 420$ nm). The MOF chosen for this work was MIL-125-NH_2, a known and stable photocatalyst. MIL-125-NH_2 absorbs light in the visible region of the solar spectrum; it can efficiently transport electrons to the crystal surface and transfer them to the co-catalyst.[10a, 15c] The photocatalytic performance of systems containing different transition metal based co-catalysts physically mixed with MIL-125-NH_2 was investigated. As a proof-of-concept, we demonstrated that the electron donor can be replaced with an organic dye in a system that delivers simultaneous photocatalytic H_2 generation and dye degradation under deaerated conditions. For this study, Rhodamine B (RhB) was chosen as a representative of organic pollutants in waste-water, as it is a hazardous dye widely used in cosmetic, textile, paint and plastic industry.[17] It exhibits high toxicity and stability and its presence in water can result in teratogenic and carcinogenic effects on public health.[18]
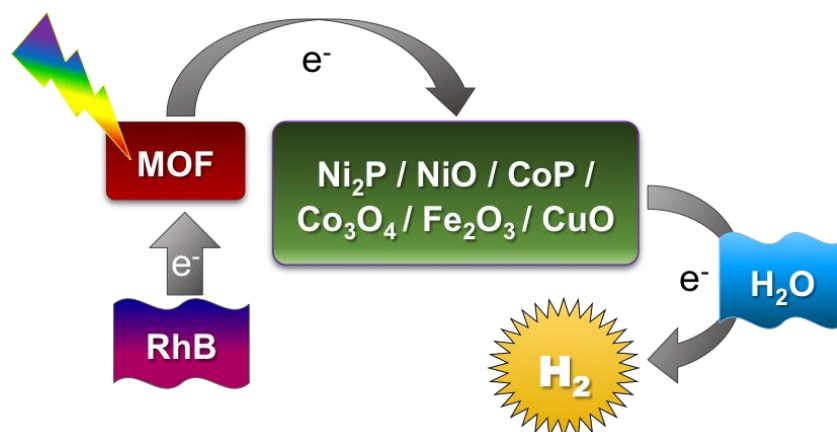
Scheme 1: Schematic representation of the strategy followed in this work: Step 1: use of different co-catalysts, Step 2: variation of the electron donors and Step 3: replacement of the electron donor with Rhodamine B (RhB), a dye that is used as a simulant organic pollutant.

2. Results and Discussion

2.1 Synthesis and Characterization

MIL-125-NH$_2$ was synthesised and characterised by means of powder X-ray diffraction (PXRD), nitrogen adsorption-desorption isotherms, scanning electron microscopy (SEM) and UV-vis absorption spectroscopy. The PXRD pattern of the bulk MIL-125-NH$_2$ is in great agreement with the pattern derived from the single-crystal structure (Figure S1a). The nitrogen isotherms performed at 77 K revealed the microporous nature of the MIL-125-NH$_2$, with a BET surface area of ~1200 m^2 g^{-1} (Figure S1b). The MIL-125-NH$_2$ crystals displayed a circular disc type morphology with a mean particle size of around 1 μm, as illustrated by the SEM images (Figure S1c). The UV-vis absorbance spectrum of the free ligand NH$_2$-H$_2$BDC (Figure S2a) and the Kubelka-Munk representation of the UV-vis diffuse reflectance spectrum of MIL-125-NH$_2$ (Figure S2b), indicate that the latter exhibits a red shift. This red shift leads to a strong absorption in the 300-480 nm range and is ascribed to the ligand-to-metal charge transfer (LMCT).[10a]

A range of transition metal phosphide and oxide co-catalysts (Ni$_2$P, NiO, CoP, Co$_3$O$_4$, Fe$_2$O$_3$ and CuO) was selected, based on their availability and low cost compared to noble-metal nanoparticles, which are commonly used in photocatalytic water splitting.[11b, 11c] The selected co-catalysts were synthesised based on a MOF-derived technique.[19] When this synthetic method is used, the self-sacrificing MOF acts as a structure directing template allowing for a more rational preparation of active NPs.[20] Specifically, the use of MOFs as precursors can yield in the generation of nano-sized materials, with higher specific surface areas, thermal stability and catalytic activity.[21] For example, Yu *et al.* developed an efficient electrocatalyst through an easy and scalable one-pot thermal treatment of bimetallic zeolitic imidazolate frameworks (ZIFs).[22]

The formation, phase purity and morphology of the MOF-derived NPs were explored through PXRD, nitrogen isotherms and transmission electron microscopy (TEM) (see section S2). The PXRD patterns of the as-synthesised NiO, Ni_2P, Co_3O_4, CoP, Fe_2O_3 and CuO NPs are in good agreement with the simulated and previously reported patterns (Figure 1).[23] The TEM images revealed the morphology and size of these NPs; the NiO, Ni_2P, Co_3O_4, and CuO NPs illustrated a spherical shape with a mean size of 10 – 20 nm, whereas Fe_2O_3 NPs had a size of 200 nm. The dimensions of the rod-shaped CoP NPs were approximately 20 nm x 6 nm (Figure S4), which is in agreement with previous reports of MOF-derived CoP NPs.[24]
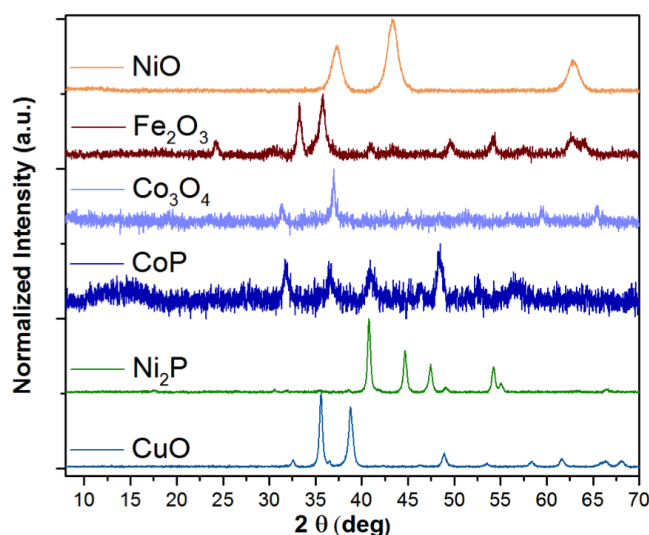
Figure 1: Powder X-ray diffraction patterns of MOF-derived NiO, Fe_2O_3, Co_3O_4, CoP, Ni_2P and CuO NPs.

2.2 Photocatalytic Performance

2.2.1 Exploration of Different Co-catalysts

In order to assess the photocatalytic performance of the different co-catalyst/MIL-125-NH_2 systems, the crystalline powder of MIL-125-NH_2 was physically mixed with varying amounts of the co-catalyst NPs. Such simple incorporation of the co-catalyst NPs (physical mixture) is advantageous, considering that complicated steps are prevented (e.g. photodeposition[11b, 25] or encapsulation[26]) and the loaded amounts of the co-catalysts are highly reproducible and controllable. The ratio between the co-catalyst NPs and the MIL-125-

NH$_2$ is crucial, since there is a volcano-type trend between the adding amount of a given co-catalyst and the photocatalytic activity of a system. In principle, the addition of the co-catalyst increases the production of H$_2$, since these NPs play a key role in facilitating the electron-hole separation within the MIL-125-NH$_2$. However, as displayed in Figure S5, further increase in the amount of the co-catalyst decreases the photocatalytic performance of the system. This is attributed to the fact that an excess amount of the co-catalyst leads to restricted penetration of the incident light in the photocatalytic solution, and can hinder the contact between MIL-125-NH$_2$ and the electron donor.[4a]

The photocatalytic solution used for these experiments included acetonitrile (CH$_3$CN), triethylamine (TEA) as the electron donor and water in a volumetric ratio of 79: 16: 5 v/v/v, respectively.[10a] As shown in Figure S5 the optimal amounts of each co-catalyst, i.e. the amount that produced the highest H$_2$ evolution rate, varied within the range of 7.9 - 10.2 wt%. Interestingly, as illustrated in Figure 2 the optimised Ni$_2$P/MIL-125-NH$_2$ photocatalytic system displayed the highest hydrogen evolution rate of 1230 μmol h^{-1} g^{-1} (over 8 h), followed by NiO/MIL-125-NH$_2$, which exhibited a rate of 1084 μmol h^{-1} g^{-1}. The performance of the Co$_3$O$_4$/MIL-125-NH$_2$ and CoP/MIL-125-NH$_2$ systems was comparable. The optimised Fe$_2$O$_3$/MIL-125-NH$_2$ system displayed a H$_2$ evolution rate of 435 μmol h^{-1} g^{-1}, followed by the CuO/MIL-125-NH$_2$ system which exhibited the lowest rate of 139 μmol h^{-1} g^{-1}. It is worth mentioning that when only the co-catalysts were subjected to photocatalytic test only traces of H$_2$ was detected (Table S1). Likewise, without any co-catalysts, MIL-125-NH$_2$ exhibits a very low H$_2$ evolution rate of ~2.25 μmol h^{-1} g^{-1}.[10a] The significantly inferior performance of solely the MIL-125-NH$_2$ highlights that the incorporation of the co-catalysts in the system remarkably promotes the H$_2$ evolution rate.
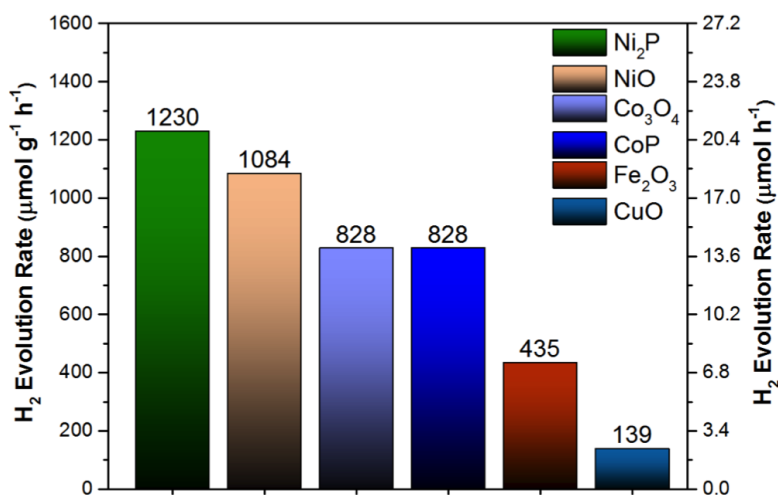
Figure 2: Comparison of H$_2$ evolution rates (with respect to MIL-125-NH$_2$) of 9.2 wt% Ni$_2$P/MIL-125-NH$_2$, 8.6 wt% NiO/MIL-125-NH$_2$, 7.9 wt% Co$_3$O$_4$/MIL-125-NH$_2$, 8.8 wt% CoP/MIL-125-NH$_2$, 10.2 wt% Fe$_2$O$_3$/MIL-125-NH$_2$ and 7.9 wt% CuO/MIL-125-NH$_2$ under visible light irradiation for 8 hours.

After the photocatalytic test the stability of both MIL-125-NH$_2$ and transition metal-based co-catalysts was assessed by means of PXRD, X-ray photoelectron spectroscopy (XPS) and SEM mapping (see section S4). Figure S6 shows that the MIL-125-NH$_2$, NiO, Co$_3$O$_4$, Fe$_2$O$_3$ and Ni$_2$P NPs retained their crystallinity after the photocatalytic water reduction reaction. XPS measurements were carried out for the CuO/MIL-125-NH$_2$ and CoP/MIL-125-NH$_2$ systems, since the characteristic Bragg reflections of CuO and CoP NPs were not apparent in the PXRD patterns due to their low concentration and crystallinity compared to the amount of MIL-125-NH$_2$ used. The Cu and Co 2p peaks were characteristic of Cu(II) and Co(III) respectively, and showed no significant change after the photocatalytic test (Figure S7). The SEM mapping images of each co-catalyst/MIL-125-NH$_2$ system after the photocatalytic test confirmed that all co-catalyst NPs were homogeneously distributed over the MIL-125-NH$_2$ crystals (Figure 3 and Figure S8). Furthermore, the N$_2$ adsorption-desorption isotherms collected on the best-performing Ni$_2$P/MIL-125-NH$_2$ and NiO/MIL-125-NH$_2$ systems before and after the photocatalytic experiments showed comparable BET surface

areas, demonstrating the retention of the porous structure of MIL125-NH$_2$ (figure S9). Recycling experiments for three consecutive cycles of 12 hours were performed on both Ni$_2$P/MIL-125-NH$_2$ and NiO/MIL-125-NH$_2$ systems (see section S5). As can be seen in figures S10 and S11, the photocatalytic activity and the crystallinity of MIL-125-NH$_2$, Ni$_2$P and NiO were retained throughout the cycles.

The majority of the investigated systems in this study outperform other systems based on MIL-125-NH$_2$ with noble metal co-catalysts such as Pt and Au NPs.[11b, 27] There are very few examples of noble metal free MIL-125-NH$_2$-based photocatalytic systems tested towards H$_2$ evolution. Among them, Gascon and co-workers reported the photocatalytic performance of a MIL-125-NH$_2$-based composite integrating a Co-dioxime-diimine complex into the pores.[15c] However, the performance of this system is inferior compared to MIL-125-NH$_2$ combined with Ni$_2$P, NiO, CoP and Co$_3$O$_4$ NPs. In addition to these co-catalyst NPs, several other (semi)conductors such as ZnIn$_2$S$_4$ or graphene were also utilized with MIL-125-NH$_2$ to boost the H$_2$ evolution rate of the system, but since they are used in high weight percentages (>50 %), they are not considered as co-catalysts.[28]
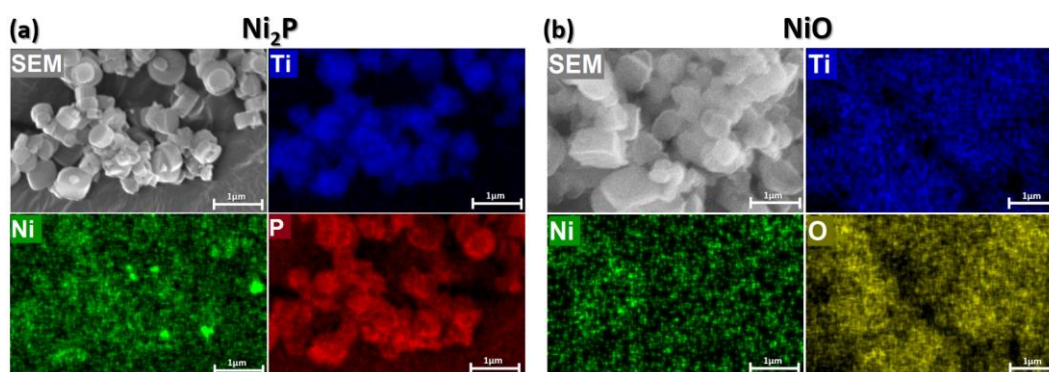
Figure 3: (a) SEM image of Ni$_2$P/MIL-125-NH$_2$ after 8-hour photocatalytic test and the corresponding EDX maps of Titanium, Nickel and Phosphorus and (b) SEM image of NiO/MIL-125-NH$_2$ after 8-hour photocatalytic test and the corresponding EDX maps of Titanium, Nickel and Oxygen. Scale bar: 1 μm.

In order to obtain further insights into the charge separation efficiency and the synergy between the MIL-125-NH$_2$ and the different co-catalysts, photoluminescence (PL) and transient PL experiments for each co-catalyst/MIL-125-NH$_2$ system were performed (see section S6). In principle, the addition of the co-catalyst NPs can quench the emission of the photocatalyst, since the NPs withdraw the photoexcited electrons and thus prevent the undesired electron-hole recombination. In preparation for the PL experiments, MIL-125-NH$_2$ was mixed with different amounts of co-catalyst NPs and the mixtures were subsequently suspended in the photocatalytic solution. To assess how efficiently each co-catalyst inhibits the electron-hole recombination, the emission quenching was quantified by integrating the PL curves of the MIL-125-NH$_2$ and the samples with the optimal amount of each co-catalyst, PL$_{co\text{-}cats}$/PL$_{MOF}$ (Table 1). The charge separation efficiency followed the order: Ni$_2$P > CoP $\approx$ Co$_3$O$_4$ > Fe$_2$O$_3$ > CuO > NiO. The PL results are consistent with the photocatalytic performance (H$_2$ generation rates) of each system, apart from the NiO/MIL-125-NH$_2$ system. As can be seen in Figure 4, the NiO NPs were less efficient at attracting the photogenerated electrons, yet this system exhibited one of the highest photocatalytic H$_2$ generation rates.
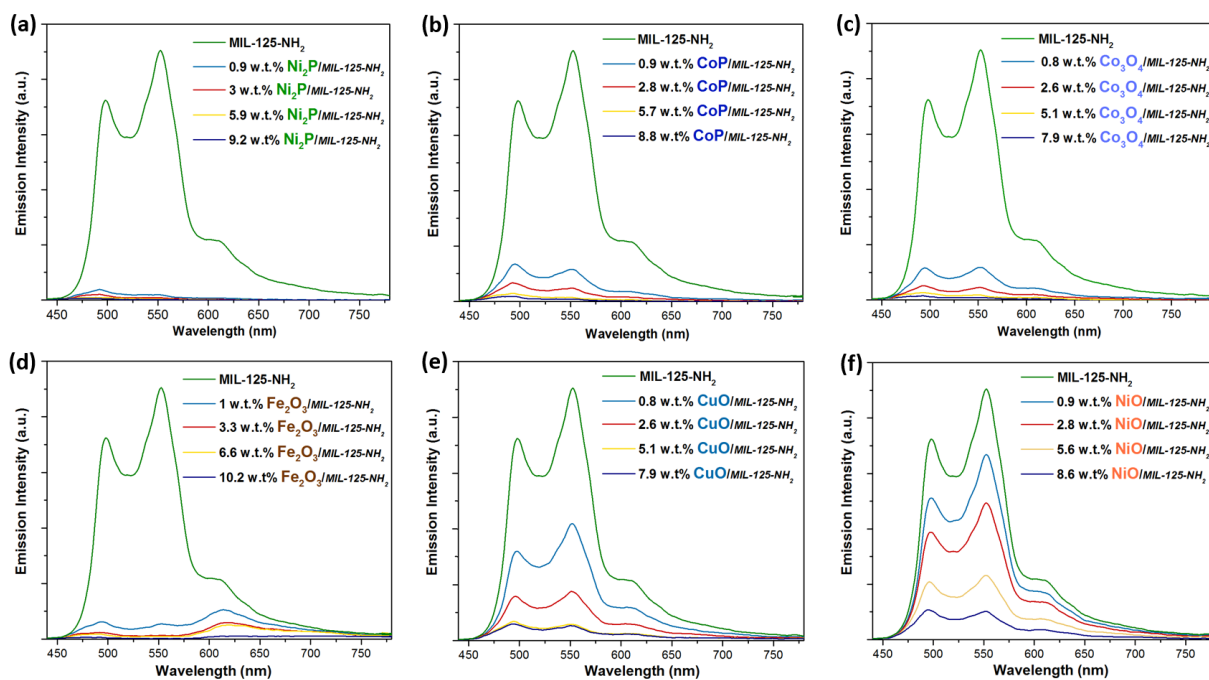
Figure 4: PL spectra of the suspensions of MIL-125-NH$_2$ with different amounts of: (a) Ni$_2$P, (b) CoP, (c) Co$_3$O$_4$, (d) Fe$_2$O$_3$, (e) CuO and (f) NiO. The co-catalyst-induced quench in the PL follows the descending order of Ni$_2$P > CoP ≈ Co$_3$O$_4$ > Fe$_2$O$_3$ > CuO > NiO. The excitation wavelength was 420 nm.

Table 1: Photoluminescent emission quench (PL$_{co-cat}$/PL$_{MOF}$) for different co-catalysts.

Co-catalyst	Ni$_2$P	CoP	Co$_3$O$_4$	Fe$_2$O$_3$	CuO	NiO
PL$_{co-cat.}$/PL$_{MOF}$, %	0.7	2.6	2.5	6	17.2	28.8

In order to gain a better understanding of the discrepancy between the PL results and the photocatalytic H$_2$ generation rate of the NiO/MIL-125-NH$_2$ system, electrochemical measurements were performed (cyclic voltammetry, CV and linear scan voltammetry, LSV). The intrinsic activity of NiO in catalyzing the H$_2$ evolution reaction was determined and compared with that of Ni$_2$P NPs (see section S7). The intrinsic catalytic activities of the co-catalysts were compared in terms of current density. To ensure that the conditions of the electrochemical experiments were comparable to those applied in photocatalysis, a solution containing acetonitrile and water (90:10) was used, with 0.1 M tetrabutylammonium

perchlorate (TBAP), to ensure the availability of conductive ions in the electrolyte. It was established that the current density (intrinsic catalytic activity) of NiO NPs was notably higher than that of the Ni$_2$P NPs (e.g. -0.22 and -0.07 mA cm^{-2} for NiO and Ni$_2$P, respectively at -0.9 V versus Ag/Ag$^+$), compensating for the inferior performance of NiO in withdrawing electrons (Figure S14). Hence, the good photocatalytic performance of the NiO/MIL-125-NH$_2$ system with respect to H$_2$ generation can be attributed to the superior intrinsic activity of NiO in catalyzing the reduction of protons to H$_2$.

From this study it is apparent that the photocatalytic performance of a system is influenced not only by the individual performance of the MOF (in terms of light absorption and charge separation within the structure) or the co-catalyst (in terms of intrinsic catalytic activity), but is also highly determined by the synergy between these two components. The last step of H$_2$ formation and desorption is associated solely with the intrinsic catalytic activity of the co-catalyst. However, despite the importance of high intrinsic activity, the last step cannot take place if there is no efficient means of transporting electrons from the MOF to the co-catalyst.

The literature contains many examples of visible light-active MOFs whose photocatalytic activity could be substantially improved by careful selection of an appropriate co-catalyst.[10a, 11b, 11c, 14e] The criteria for the co-catalyst selection should relate mainly to the synergy with the photocatalyst, rather than to its intrinsic catalytic activity. The target of this strategy is to achieve efficient interactions between the two components, ensuring efficient migration of electrons from the MOF to the co-catalyst. Transition metal phosphides and oxides have emerged as promising co-catalysts for H$_2$ evolution reaction and their use in MOF-based photocatalytic systems can lead to performances similar to those achieved with traditional semiconductors.

2.2.2 Investigation of Different Electron Donors

The sacrificial electron donor is another crucial component in a photocatalytic system. An efficient electron donor should exhibit thermodynamic adequacy with the photocatalyst, irreversible transformation into inert molecules and fast kinetics of oxidation.[29] Depending on individual photocatalytic systems, other potentially desirable electron donor characteristics include stability across a certain pH range, diffusibility into the pores of the photocatalyst, and being used in high concentrations without causing any degradation or collapse to the other components present in the system (e.g. photocatalyst, co-catalyst). In this section, we describe the photocatalytic performance of the $Ni_2P/MIL-125-NH_2$ system with different sacrificial reagents as electron donors. In addition to TEA, four other commonly used electron donors – L-ascorbic acid (H_2A), methanol (MeOH), ethanol (EtOH), and triethanolamine (TEOA), were investigated.[30] The amount of water was kept constant at 5% v/v in all the examined photocatalytic solutions (Section S8).

Varying the electron donor had a profound impact on the H_2 production rate (Figure 5a). Using TEA and TEOA promoted the H_2 generation, however the H_2 evolution rate in the case of TEOA was ~6 times lower than that when TEA was employed (215 vs. 1230 $\mu mol\ h^{-1}\ g^{-1}$). When EtOH or MeOH were employed, the $Ni_2P/MIL-125-NH_2$ system exhibited remarkably inferior activity, with H_2 evolution rates of only 38 and 26 $\mu mol\ h^{-1}\ g^{-1}$ for EtOH and MeOH, respectively. When L-ascorbic acid was used as the electron donor no H_2 evolution was observed. Both Ni_2P and $MIL-125-NH_2$ retained their stability after all these photocatalytic tests (Figure 5b). The inactivity of L-ascorbic acid was expected since the photocatalytic solution contained mainly acetonitrile, which is a much less polar solvent than water and therefore inhibits the dissociation of H_2A into HA^- and the subsequent oxidation of HA^- to $HA^{\bullet}$ as in aqueous media. EtOH and MeOH are weaker bases than TEA and TEOA, which may explain why they were less effective electron donors.
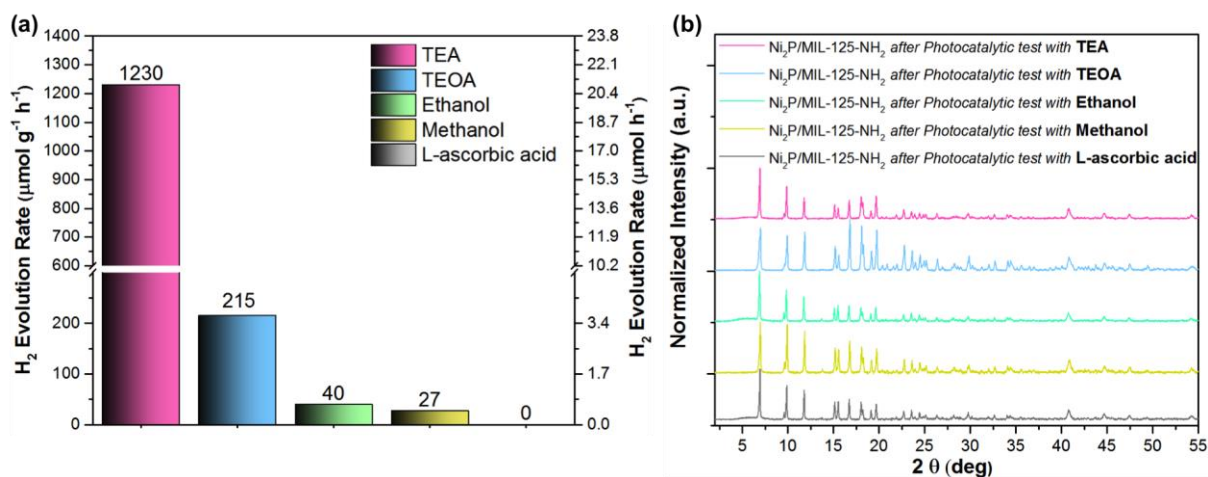
Figure 5: (a) Comparison of H$_2$ evolution rates of 9.2 wt% Ni$_2$P/MIL-125-NH$_2$ with different electron donors, under visible light irradiation for 8 h, (b) Powder x-ray diffraction patterns of 9.2 wt% Ni$_2$P/MIL-125-NH$_2$ after the photocatalytic test with different electron donors.

Given the requirements of photocatalysis, that the electron transfer process should be faster than the charge recombination and that the same number of electrons and holes are to be used, the rate of the oxidation reaction of the electron donors should be sufficiently high so as not to slow down the water reduction process. It appears that the oxidation of EtOH and MeOH is not adequate within the Ni$_2$P/MIL-125-NH$_2$ system, leading to the inferior performance of these photocatalytic systems. Finally, the higher H$_2$ evolution rate of the photocatalytic system with TEA compared to that with TEOA can be attributed to the difference in the concentrations used (TEA: 1.18 M, TEOA: 0.01 M). This effect can also be observed from the cyclic voltamograms (CV) of TEA and TEOA at these concentrations (section S8.1). As can be seen in Figure S15, when scanned toward positive potential, the current density of the anodic peak with TEA (onset at 1.4 V vs. Ag/Ag$^+$) is an order of magnitude higher than that of TEOA (and the other electron donors). In principle, the current density should be proportional to the rate of oxidation and the concentration of the electron donors. This indicates that even if the oxidation of TEA and TEOA occurs at comparable rates, the ability to use a much higher concentration of TEA with the Ni$_2$P/MIL-125-NH$_2$

system is important for the efficiency of the electron donation process. It is worth noting that we attempted to increase the concentration of TEOA in the photocatalytic system, but this led to the partial or complete degradation of MIL-125-NH$_2$.

2.2.3 Dual Photocatalytic Activity

As the above results demonstrate, using electron donors can favourably influence the H$_2$ generation performance of a photocatalytic system. Nevertheless, incorporating electron donors into a photocatalytic system inhibits its industrial application, mainly due to their cost and toxicity (in the case of TEA, TEOA, and MeOH). In an attempt to address these limitations and provide a proof-of-concept for an alternative approach, we explored a system in which the electron donor was replaced by a typical organic pollutant, envisioning H$_2$ generation coupled with water remediation.

The main photoactive species required for dye photodegradation can be complementary to those needed for the photocatalytic H$_2$ evolution reaction (holes for the former and electrons for the latter). The challenge of combining these two reactions lies in the fact that the photocatalytic H$_2$ production is unlikely to occur in aerated conditions, since O$_2$ acts as an electron scavenger, whereas the photocatalytic oxidation of organic pollutants is significantly promoted in the presence of O$_2$. Hence, the photocatalyst should be capable of degrading the organic pollutant with the holes being the dominant photoactive species and the electrons being transferred to protons (H$^+$) or water molecules to generate H$_2$.

This idea was explored by using the optimum 9.2 wt% Ni$_2$P/MIL-125-NH$_2$ system due to the strong synergy of MIL-125-NH$_2$ crystals with the Ni$_2$P NPs towards the photocatalytic H$_2$ generation. The organic pollutant used in this study was Rhodamine B (RhB), a dye whose photocatalytic degradation has been extensively studied with MOFs.[31] The RhB concentration was varied in the CH$_3$CN-based solution with water, in order to identify the favourable conditions for H$_2$ production. As illustrated in Figure 6a and S16a, when the dye

concentration initially increases, the H_2 evolution rate is promoted, indicating that more RhB molecules are available to interact with the photoexcited holes. Further increase in RhB concentration causes a decrease in the amount of H_2 generated, since a portion of the incident light is inhibited from approaching the MIL-125-NH$_2$. The H_2 evolution rate reached a maximum value of 335 μmol h^{-1} g^{-1} at a RhB concentration of 1.2 ppm in the photocatalytic solution (0.02 mg in 17 mL). The H_2 evolution rate was found to be lower when RhB was used as an electron donor than when TEA was used. This is in accordance with the basicity of these substances and the fact that the TEA concentration used was significantly higher than that of RhB. In addition, the smaller size of the TEA molecules could allow them for more efficient diffusion through the porous assemblies of MIL-125-NH$_2$, and thus provide more effective electron donation. The overall advantage of using RhB as an electron donor relies on the significant benefit of dual-function photocatalysis.
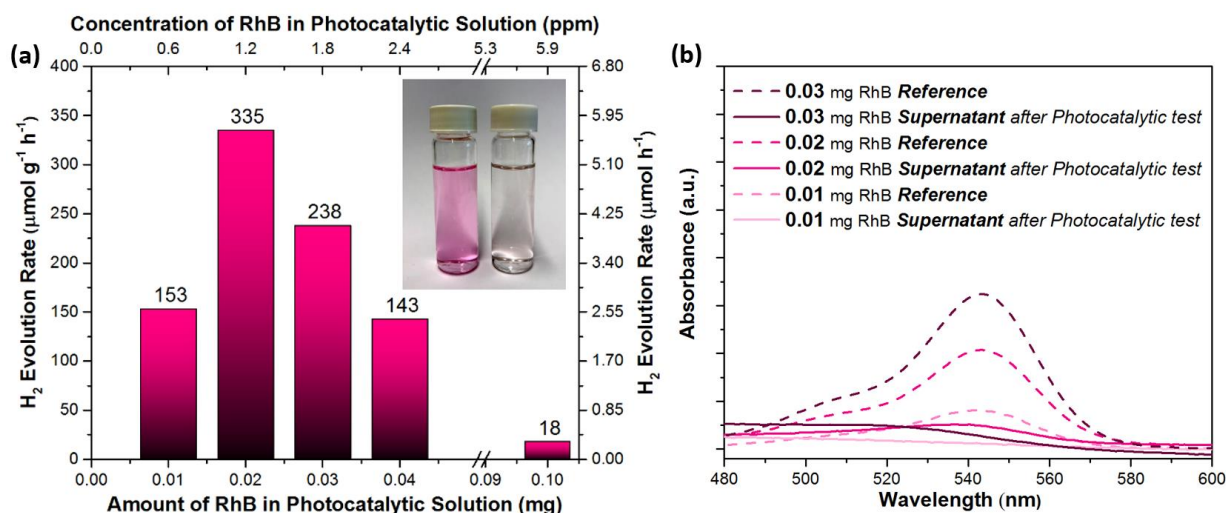
Figure 6: (a) Photocatalytic H_2 evolution rates of 9.2 wt% Ni$_2$P/MIL-125-NH$_2$ in 17 mL of photocatalytic solutions with different concentration of RhB under visible light irradiation for 8 h. Inset: a photograph showing the difference in the color of the 1.2 ppm solution before and after the photocatalytic test with Ni$_2$P/MIL-125-NH$_2$. (b) UV-Vis spectra of reference samples and supernatants after the photocatalytic RhB decolorization process.

After the photocatalytic test, the RhB concentration was monitored for the three best performing solutions (initial RhB concentration of 0.6, 1.2 and 1.8 ppm, Figure 6b). For this purpose, the UV-Vis absorbance spectra of the supernatants after the photocatalytic test were collected. With an initial RhB concentration of 0.6 ppm, the dye was completely degraded and with concentration of 1.2-1.8 ppm, the dye concentration decreased substantially. Control experiments were performed to confirm that RhB was photodegraded and not absorbed by MIL-125-NH$_2$. The Ni$_2$P/MIL-125-NH$_2$ system was immersed in 1.2 ppm RhB solution and kept in the dark for 24 h. The supernatant was then collected and subjected to UV-vis spectroscopy. Interestingly, there was no notable difference between the RhB concentrations before and after this test (Figure S17a). Moreover, when 1.2 ppm RhB solution was irradiated in the absence of MIL-125-NH$_2$, there was no change in the dye concentration, confirming that no self-photolysis of RhB occurs (Figure S17b). These results indicate that RhB is indeed involved in the photocatalytic process of H$_2$ evolution.
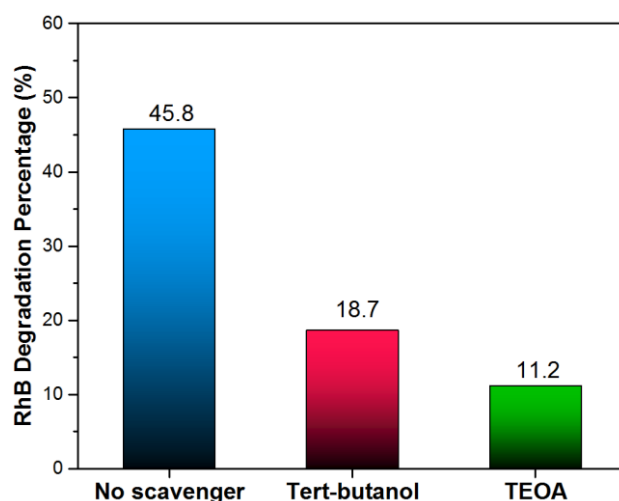
Figure 7: The impact of the incorporation of TEOA as hole scavenger, tert-butanol as •OH radical scavenger, or no scavenger on the RhB degradation rate after 3 h photocatalytic test.

To provide further confirmation of the role of RhB and elucidate the photocatalytic mechanism, trapping experiments of active species were carried out using the optimal RhB

concentration (1.2 ppm, 2.5 μM) and 0.01 M tert-Butanol as •OH radical scavenger or 0.01 M

TEOA as hole scavenger (Figure S18a). As displayed in Figure 7, the addition of TEOA and

tert-Butanol led to 11.2 % and 18.7 % decrease in the RhB concentration, respectively. This

confirms that both the holes and •OH radicals are involved in this process, with the former

being the more dominant species. These results further prove that RhB acts as a sacrificial

electron donor, scavenging the photoexcited holes and promoting the H_2 generation, which

leads to its decomposition, as demonstrated by UV-Vis spectroscopy (Figure 6b).

Recently, Cho *et al.* and Kim *et al.* have also investigated the dual functional

photocatalysis for H_2 production with simultaneous degradation of 4-chlorophenol and urea,

urine and 4-chlorophenol, respectively.[16] These photocatalytic systems however are based on

wide band gap semiconductors such as $SrTiO_3$ and TiO_2 and noble metals NPs (e.g. Rh, Pt) as

co-catalysts. In our work, the photocatalytic systems operate under visible light irradiation

which constitutes ~44% of the solar spectrum and are free of noble metals.

3. Conclusions

In summary, we investigated the H_2 generation performance of several photocatalytic

systems based on MIL-125-NH_2 combined with a wide range of abundant co-catalysts and

electron donors. The variation in performance depending on the choice of co-catalyst

highlights the key role of these NPs in promoting the H_2 evolution reaction and demonstrates

that earth-abundant, cost-effective co-catalysts can challenge the commonly used noble metal

NPs, such as Pt. The photocatalytic system with TEA as electron donor and Ni_2P or NiO as

co-catalyst demonstrated among the highest H_2 evolution rates for MOFs. The high

photocatalytic activity of these systems can be attributed to the exceptional synergy between

the MIL-125-NH_2 and the co-catalyst NPs, the compatibility between the MIL-125-NH_2 and

TEA and the fast kinetics of the TEA oxidation process.

Drawing on these insights, we then integrated the photocatalytic H_2 evolution and

degradation of the organic dye RhB in a single process using the Ni_2P/MIL-125-NH_2 system

under deaerated conditions. This dual-functional photocatalytic system generated H_2 at a relatively high rate and the organic dye acting as an electron donor was degraded under visible-light irradiation. To the best of our knowledge this is the first example of a dual-functional MOF-based photocatalytic system that simultaneously produces H_2 and degrades organic pollutants under visible light irradiation. This study showcases the great potential of MOFs in photocatalytic applications and paves the way for the generation of new visible light-active and water-stable MOF-photocatalysts that can accomplish simultaneous water remediation and H_2 generation.

Supporting Information

General methods, synthetic procedures, characterization details, SEM, TEM, transient photoluminescence and electrochemical experiments are shown within the supporting information.

Acknowledgements

Conflict of interest

KCS, SK, TNN, BS and EPFL have filed a patent application (EP17180055.0) that relates to visible light-active Ti-MOFs and cheap co-catalysts for photocatalytic water splitting and H_2 generation.

References

[1]   a) F. E. Osterloh, *Chem. Mater.* **2008**, 20, 35; b) A. Mills, S. Le Hunte, *J. Photochem. Photobiol. A* **1997**, 108, 1; c) T. Zhang, W. Lin, *Chem. Soc. Rev.* **2014**, 43, 5982.

[2]   a) U. I. Gaya, A. H. Abdullah, *J. Photochem. Photobiol., C* **2008**, 9, 1; b) X. Chen, S. Shen, L. Guo, S. S. Mao, *Chem. Rev.* **2010**, 110, 6503.

[3]   C. K. C., F. Paolo, *Chem. Cat. Chem.* **2017**, 9, 1523.

[4]   a) J. Ran, J. Zhang, J. Yu, M. Jaroniec, S. Z. Qiao, *Chem. Soc. Rev.* **2014**, 43, 7787; b) X. Zou, Y. Zhang, *Chem. Soc. Rev.* **2015**, 44, 5148; c) A. Schoedel, Z. Ji, O. M. Yaghi, *Nat Energy* **2016**, 1.

[5]   D. Chatterjee, S. Dasgupta, *J. Photochem. Photobiol., C* **2005**, 6, 186.

[6]   D. Seckler, R. Barker, U. Amarasinghe, *Int. J. Water Res.* **1999**, 15, 29.

[7]   A. Ajmal, I. Majeed, R. N. Malik, H. Idriss, M. A. Nadeem, *RSC Adv.* **2014**, 4, 37003.

[8]   S. Wang, X. Wang, *Small* **2015**, 11, 3097.

[9]   M. Hayyan, M. A. Hashim, I. M. AlNashef, *Chem. Rev.* **2016**, 116, 3029.

[10]   a) S. Kampouri, T. N. Nguyen, C. P. Ireland, B. Valizadeh, F. M. Ebrahim, G. Capano, D. Ongari, A. Mace, N. Guijarro, K. Sivula, A. Sienkiewicz, L. Forro, B. Smit, K. C. Stylianou, *J. Mater. Chem. A* **2018**, 6, 2476; b) W.-Z. Gao, Y. Xu, Y. Chen, W.-F. Fu, *Chem. Commun.* **2015**, 51, 13217.

[11]   a) J.-J. Zou, H. He, L. Cui, H.-Y. Du, *Int. J. Hydrogen Energy* **2007**, 32, 1762; b) Y. Horiuchi, T. Toyao, M. Saito, K. Mochizuki, M. Iwata, H. Higashimura, M. Anpo, M. Matsuoka, *J. Phys. Chem. C* **2012**, 116, 20848; c) A. Fateeva, P. A. Chater, C. P.

Ireland, A. A. Tahir, Y. Z. Khimyak, P. V. Wiper, J. R. Darwent, M. J. Rosseinsky, *Angew. Chem. Int. Ed.* **2012**, 51, 7440.

[12] a) A. G. Tamirat, J. Rick, A. A. Dubale, W.-N. Su, B.-J. Hwang, *Nanoscale Horiz.* **2016**, 1, 243; b) W. Wang, X. Xu, W. Zhou, Z. Shao, *Advanced Science* **2017**, 4, 1600371.

[13] a) S. L. Anderson, K. C. Stylianou, *Coord. Chem. Rev.* **2017**, 349, 102; b) H. Furukawa, K. E. Cordova, M. O'Keeffe, O. M. Yaghi, *Science* **2013**, 341; c) S. M. Cohen, *Chem. Rev.* **2012**, 112, 970.

[14] a) M. Ranocchiari, J. A. van Bokhoven, *Phys. Chem. Chem. Phys.* **2011**, 13, 6388; b) M. A. Nasalevich, C. H. Hendon, J. G. Santaclara, K. Svane, B. van der Linden, S. L. Veber, M. V. Fedin, A. J. Houtepen, M. A. van der Veen, F. Kapteijn, A. Walsh, J. Gascon, **2016**, 6, 23676; c) J. G. Santaclara, F. Kapteijn, J. Gascon, M. A. van der Veen, *Cryst. Eng. Comm.* **2017**, 19, 4118; d) J. G. Santaclara, M. A. Nasalevich, S. Castellanos, W. H. Evers, F. C. M. Spoor, K. Rock, L. D. A. Siebbeles, F. Kapteijn, F. Grozema, A. Houtepen, J. Gascon, J. Hunger, M. A. van der Veen, *Chem. Sus. Chem.* **2016**, 9, 388; e) F. Xinzuo, S. Qichao, W. Yu, J. Long, Y. Tao, L. Yafei, Z. Qun, L. Yi, J. Hai‑Long, *Adv. Mater.* **2018**, 30, 1705112; f) L. Hang, X. Caiyun, L. Dandan, J. Hai‑Long, *Angew. Chem. Int. Ed.* **2018**, 57, 5379; g) C. H. Hendon, D. Tiana, M. Fontecave, C. Sanchez, L. D'arras, C. Sassoye, L. Rozes, C. Mellot-Draznieks, A. Walsh, *J. Am. Chem. Soc.* **2013**, 135, 10942; h) S. Pullen, H. Fei, A. Orthaber, S. M. Cohen, S. Ott, *J. Am. Chem. Soc.* **2013**, 135, 16997; i) E. M. Dias, C. Petit, *J. Mater. Chem. A* **2015**, 3, 22484.

[15] a) X.-Y. Dong, M. Zhang, R.-B. Pei, Q. Wang, D.-H. Wei, S.-Q. Zang, Y.-T. Fan, T. C. W. Mak, *Angew. Chem. Int. Ed.* **2016**, 55, 2073; b) T. Toyao, M. Saito, S. Dohshi, K. Mochizuki, M. Iwata, H. Higashimura, Y. Horiuchi, M. Matsuoka, *Chem. Commun.*

2014, 50, 6779; c) M. A. Nasalevich, R. Becker, E. V. Ramos-Fernandez, S. Castellanos, S. L. Veber, M. V. Fedin, F. Kapteijn, J. N. H. Reek, J. I. van der Vlugt, J. Gascon, *Energy Environ. Sci.* **2015**, 8, 364; d) C. Wang, K. E. deKrafft, W. Lin, *J. Am. Chem. Soc.* **2012**, 134, 7211; e) S. Yuan, J.-S. Qin, H.-Q. Xu, J. Su, D. Rossi, Y. Chen, L. Zhang, C. Lollar, Q. Wang, H.-L. Jiang, D. H. Son, H. Xu, Z. Huang, X. Zou, H.-C. Zhou, *ACS Cent. Sci.* **2018**, 4, 105.

[16]   a) Y.-J. Cho, G.-h. Moon, T. Kanazawa, K. Maeda, W. Choi, *Chem. Commun.* **2016**, 52, 9636; b) J. Kim, D. Monllor-Satoca, W. Choi, *Energy Environ. Sci.* **2012**, 5, 7647.

[17]   a) K. Yu, S. Yang, H. He, C. Sun, C. Gu, Y. Ju, *J. Phys. Chem. A* **2009**, 113, 10024; b) M. Hassanpour, H. Safardoust-Hojaghan, M. Salavati-Niasari, *J. Mol. Liq.* **2017**, 229, 293.

[18]   a) C.-C. Wang, J.-R. Li, X.-L. Lv, Y.-Q. Zhang, G. Guo, *Energy Environ. Sci.* **2014**, 7, 2831; b) E. Baldev, D. MubarakAli, A. Ilavarasi, D. Pandiaraj, K. A. S. S. Ishack, N. Thajuddin, *Colloids Surf B Biointerfaces* **2013**, 105, 207.

[19]   D. P. Kumar, J. Choi, S. Hong, D. A. Reddy, S. Lee, T. K. Kim, *ACS Sustain. Chem. Eng.* **2016**, 4, 7158.

[20]   R. V. Jagadeesh, K. Murugesan, A. S. Alshammari, H. Neumann, M.-M. Pohl, J. Radnik, M. Beller, *Science* **2017**, DOI: 10.1126/science.aan6245.

[21]   W. Rui, D. Xi‑Yan, D. Jiao, Z. Jin‑Yan, Z. Shuang‑Quan, *Adv. Mater.* **2018**, 30, 1703711.

[22]   Z. Yu, Y. Bai, S. Zhang, Y. Liu, N. Zhang, G. Wang, J. Wei, Q. Wu, K. Sun, *ACS Appl. Mater. Interfaces* **2018**, 10, 6245.

[23]   L. Li, X. Li, L. Ai, J. Jiang, *RSC Adv.* **2015**, 5, 90265.

[24]   B. Pradhan, G. S. Kumar, A. Dalui, A. H. Khan, B. Satpati, Q. Ji, L. K. Shrestha, K. Ariga, S. Acharya, *J. Mater. Chem. C* **2016**, 4, 4967.

[25]   C. Hou, Q. Xu, Y. Wang, X. Hu, *RSC Adv.* **2013**, 3, 19820.

[26]   J.-D. Xiao, Q. Shang, Y. Xiong, Q. Zhang, Y. Luo, S.-H. Yu, H.-L. Jiang, *Angew. Chem.* **2016**, 128, 9535.

[27]   a) D. Sun, W. Liu, Y. Fu, Z. Fang, F. Sun, X. Fu, Y. Zhang, Z. Li, *Chem. Eur. J.* **2014**, 20, 4780; b) T. Toyao, M. Saito, Y. Horiuchi, K. Mochizuki, M. Iwata, H. Higashimura, M. Matsuoka, *Catal. Sci. Technol.* **2013**, 3, 2092.

[28]   a) H. Liu, J. Zhang, D. Ao, *Appl. Catal., B* **2018**, 221, 433; b) Y. Wang, Y. Yu, R. Li, H. Liu, W. Zhang, L. Ling, W. Duan, B. Liu, *J. Mater. Chem. A* **2017**, 5, 20136.

[29]   Y. Pellegrin, F. Odobel, *C. R. Chim.* **2017**, 20, 283.

[30]   a) C. Gomes Silva, I. Luz, F. X. Llabrés i Xamena, A. Corma, H. García, *Chem. Eur. J.* **2010**, 16, 11133; b) J.-J. Zhou, R. Wang, X.-L. Liu, F.-M. Peng, C.-H. Li, F. Teng, Y.-P. Yuan, *Appl. Surf. Sci.* **2015**, 346, 278.

[31]   a) H. Guo, D. Guo, Z. Zheng, W. Weng, J. Chen, *Appl. Organomet. Chem.* **2015**, 29, 618; b) Z. Sha, J. Sun, H. S. O. Chan, S. Jaenicke, J. Wu, *Chem Plus Chem* **2015**, 80, 1321; c) Q. Xia, X. Yu, H. Zhao, S. Wang, H. Wang, Z. Guo, H. Xing, *Cryst. Growth Des.* **2017**, DOI: 10.1021/acs.cgd.7b00504; d) L. Ai, C. Zhang, L. Li, J. Jiang, *Appl. Catal., B* **2014**, 148–149, 191; e) K. Fan, W.-X. Nie, L.-P. Wang, C.-H. Liao, S.-S. Bao, L.-M. Zheng, *Chem. Eur. J.* **2017**, 23, 6615.

Table of contents entry and figure.

Dual photocatalytic activity. Using a two-fold strategy, we investigated the impact of different co-catalysts and electron donors in a MOF photocatalytic system towards the water reduction. Drawing on these insights, we replaced the electron donor with an organic dye and achieved simultaneous photocatalytic hydrogen production and dye degradation.